

# Contact modelling of patterned liquid crystal polymer coatings

Frits Kernkamp

Supervised by Patrick R. Onck and Ling Liu

Micromechanics of Materials, Zernike Institute for Advanced Materials,  
University of Groningen, 9747 AG Groningen, The Netherlands

23 May 2016

## Abstract

Responsive surfaces are promising and upcoming fields which can serve as actuators and sensors in a variety of applications. Switchable surfaces with topographical transformations are specially intriguing since the surface texture changes can be utilized to dynamically control mechanical friction properties, adhesion, acoustics, optical reflections and wettability behaviors. Using responsive materials to manipulate friction is addressed in this report. In 2012 Liu and Broer have revealed a soft material based on glassy liquid crystal polymer coatings that allows light controlled friction. In their experimental implementations the friction force between two rubbing responsive coatings were measured. The friction behavior was shown to be dependent on how the two coatings were aligned against each other and was found to be anisotropic. The coating features regular corrugation profiles after light illumination. The resulting friction depends on how the regular corrugations of the two sliding coatings interact. Depending on the orientation, the friction has been shown to take values larger than, equal to and smaller than before illumination, showing a fully controllable friction behavior. The mechanism behind this is not yet fully understood. In order to explain the experimentally observed anisotropic friction coefficient in contact between two liquid crystal polymer coatings, two analytical contact problems are solved in this report. The first model which assumes rectangular, incompressible protrusions, suggests that the area of contact is independent of the angle, reducing the effective contact area to only a portion of the total apparent area. The second tested model approximates the protrusions as cylindrical objects. This model shows an angular dependence which does not mimic the experimental behaviour sufficiently. The discrepancies between the results based on the two analytical models above and the experimental results lead to a discussion related to the origin of friction on both a macroscopic level as well as a microscopic level in rough surfaces. The results presented in this report may serve as a basis for further investigation on this topic. Some suggestions are given which may be helpful to shed light on the nature of friction between polymeric materials.

# Contents

<b>1</b>	<b>Introduction</b>	<b>4</b>
<b>2</b>	<b>Experiment</b>	<b>5</b>
<b>3</b>	<b>Rigid rectangular protrusions model</b>	<b>7</b>
<b>4</b>	<b>Cylindrical protrusions model</b>	<b>11</b>
<b>5</b>	<b>Discussion</b>	<b>15</b>
5.1	Rigid rectangular protrusions model . . . . .	15
5.2	Cylindrical protrusions model . . . . .	16
5.3	Friction mechanisms . . . . .	16
5.4	Numerical model . . . . .	17
<b>6</b>	<b>Conclusion</b>	<b>18</b>

# 1 Introduction

Friction is a phenomenon which is seen almost everywhere in nature and in length scales ranging from tectonic plates to the contact of atoms<sup>[1]</sup> <sup>[2]</sup>. This subject has been thoroughly investigated over the years, in man made structures as well as in living cells<sup>[3]</sup>. However, a demand has developed for the possibility of actively altering friction and for the theory needed to describe this. The materials which are suitable for this require external triggers to induce friction change<sup>[4]</sup>. Applications for this lay in robotics<sup>[5]</sup>.

More than a century has passed since liquid crystals, were recognised as a state of matter<sup>[6]</sup>. Since then different research groups have taken interest in investigating the properties and applications of liquid crystal polymers.

Liquid crystals polymers have a large number of applications, in the fields of display technology (LCD TVs), mechanics<sup>[7]</sup>, optics and photonics<sup>[8]</sup> and others<sup>[9]</sup>. Liquid crystals with switchable surface patterning are the type that is most relevant to this paper.

The experiments of Liu and Broer in 2014<sup>[10]</sup> shows that light can be used to actuate a liquid crystal polymer coating, changing the surface structure. In the experiments two glass plates with liquid crystal coatings are slid against each other in different orientations and the friction is examined. The experiments reveal a light controlled anisotropic friction coefficient which is not yet understood.

The aim of this paper is to create a model that can explain the anisotropic friction coefficient of a liquid crystal polymer coating that has been actuated, as seen in the experiments of Liu and Broer. In the process of designing a material with desired properties, the need arises for models that can relate the microscopic properties like spacing between protrusions to macroscopically measurable quantities. In this work the friction of these surface topologies are investigated.

The process of investigating the friction coefficient has been divided into parts explained below. The experiments of Liu and Broer are first discussed in greater detail in Section 2, as these provide a basis for this paper. To see if a very simple model can explain experimental results, Section 3 of this paper focuses on the area of contact between regular spaced, rectangular protrusions. As this basic model ignores deformation, Section 4 examines the area of contact between deformable cylindrical protrusions. After this the results of both models are discussed and suggestions for further investigation are presented in Section 5, with a short conclusion in Section 6.

## 2 Experiment

In this chapter the experiments on which this report is based are described in greater detail. The pioneering work on responsive topographies of Liu and Broer<sup>[10]</sup> has led to the subject of this paper. In their experiments both static and dynamic angular friction behaviours of a liquid crystal polymer coatings with special textures are measured. The significance of the polymer layer coatings is that they have switchable surfaces, meaning that the surface structures can dynamically be altered.

Upon illumination of UV-light, the top surface of the LC coatings will form surface structures with regular corrugations, as shown in Figure 1. The deformation of the top surface depends on the illumination configuration and the molecular alignment of the liquid crystal molecules. When polymer coating is exposed to UV-light, the Homeotropic region (where the averaged LC molecules direction is parallel to the thickness direction) contracts. The Chiral-Nematic region (where the molecular directions form a helix and keep rotating along that helix) expands in the direction normal to the axis of the helix. Thus under a uniform illumination a liquid crystal coating which has periodically alternating Homeotropic region and Chiral-Nematic regions will be activated to have a regular and periodically corrugated surface.

The corrugation amplitude of the altered surface topography depends amongst others on the intensity of the input light, the material responsivity to the light stimulus, the patterned configuration and the elastic mechanical properties of the LC material. In this report the actuation and deformation of the material upon illumination are avoided, however, the surface profile after deformation is used for further investigation.

To investigate the angular behaviour of the dynamic friction coefficient, two actuated coatings are slid against each other with the corrugated sides facing each other, at an angles  $\alpha$ , ranging from  $0^\circ$  to  $90^\circ$  (for an illustration of  $\alpha$ , see Figure 2 (a)). The measured friction force is then compared to the un-activated situation in Figure 2 (d). It can be seen that orthogonal alignment results in a friction coefficient of about 50% of the flat case, whereas the friction increases to 150% for the parallel alignment.

In order to understand the angular dependence of the friction force for the regularly corrugated topographies, several explanations are proposed. It is suggested that the friction changes may be attributed to either, a change in the effective contact area, an interlocking effect, or a combination of these two depending on the length scale of the geometry. The aim of this paper is to explain the anisotropic friction curves of the actuated LC polymer coatings as seen in Figure 2 (d).

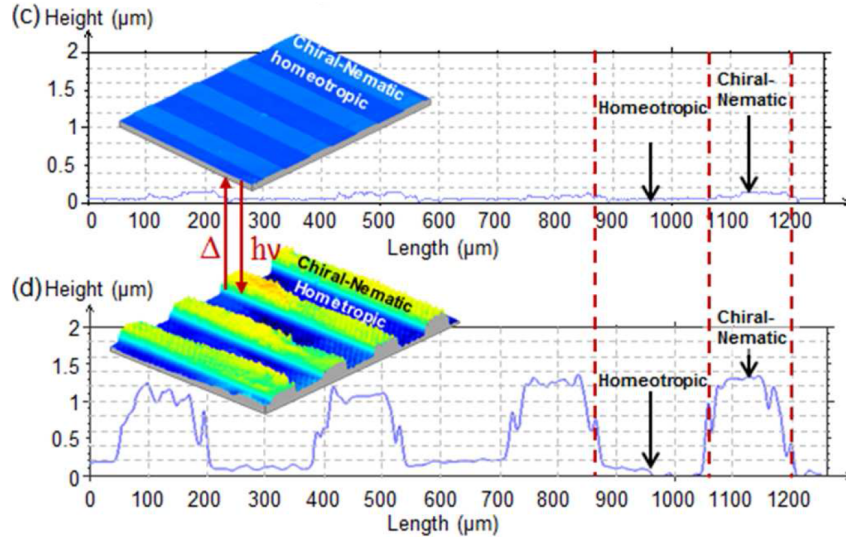


**Figure 1:** Interferometer graph of liquid crystal polymer in normal and actuated states. The Chiral-Nematic region expands upon UV illumination, whereas the homeotropic region contracts. The height/length scaling emphasizes the formation of protrusions. Because of the scaling the protrusions initially seem rectangular (for details see Section 3), however approximating the ridge as being part of a cylinder could be equally valid (see Section 4 for details).<sup>[10]</sup>

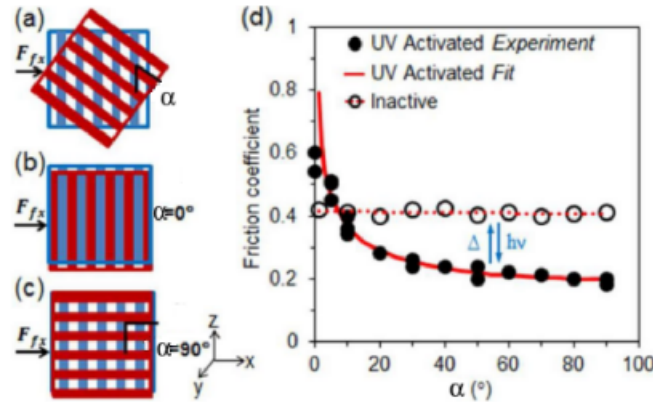


**Figure 2:** The variation of the friction behavior against the alignment angle is shown. Figure (a) Shows two LC coatings that are placed on top of each other under an angle  $\alpha$ . In Figure (b) the protrusions are aligned parallel, assumingly interlocking will now occur. Figure (c) shows the two coating structures inclined at  $\alpha = 90^\circ$ . In Figure (d) the friction coefficients are plotted as function of the angle between the two coating structures. The red line is a fitted curve for the data. <sup>[10]</sup>

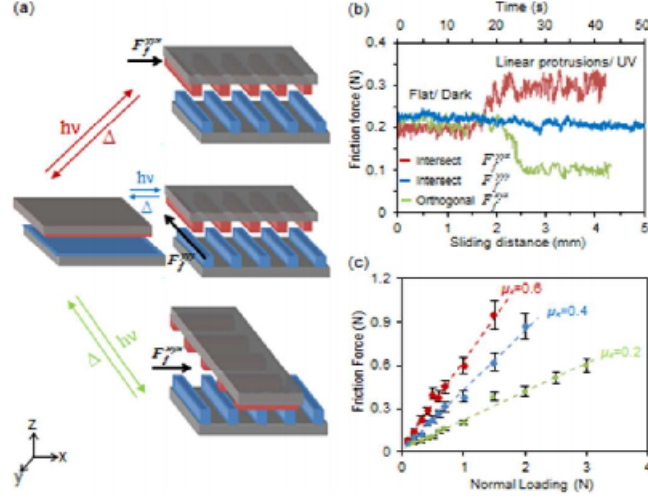


**Figure 3:** The friction dynamics when linear protrusions are formed and erased is illustrated for three exemplary cases. Figure (a) gives a schematic illustration of the sliding orientation with respect to the orientation of the formed protrusions. In Figure (b) the dynamic friction forces when the coatings undergo a transition from flat to corrugated is plotted for the three cases depicted in (a). In (c) the friction forces as function of normal loading are seen with the derived friction coefficients.<sup>[10]</sup>

### 3 Rigid rectangular protrusions model

As a first step in modelling the area of contact between two actuated liquid crystal polymer coatings a basic model is proposed, which ignores deformation. The most important assumptions are as follows: The two plates with LC polymer coatings are assumed to be identical. Each coating has a surface which is perfectly smooth. The protrusions, which are visualised in Figure 1, can be approximated as being rectangular, see Figure 4. The lengths  $a$  and  $b$  as defined in Figure 4 are assumed to be identical for each protrusion, so the coating is perfectly periodic. Finally, the normal force, acting on the two identical plates, is assumed to be uniform in the coating. These assumptions have turned the problem into a static geometry problem in which we are interested in the area of contact as a function of the angle  $\alpha$  between the protrusions. In order to calculate the contact area, a relation between the macroscopic length and the microscopic dimensions will be used. Since this problem governs dry, static friction, Amontons' law describes the relation between normal and tangential forces,

$$\mu = \frac{F_f}{F_N}. \quad (1)$$

In the equation above  $\mu$  is the friction coefficient of the material,  $F_f$  is the friction force and  $F_N$  is the normal force, which is a constant in this problem.

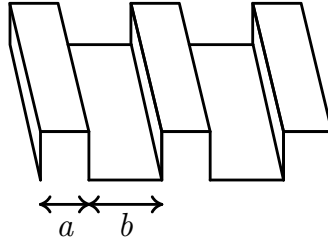


**Figure 4:** The approximation of the protrusions seen in Figure 1 is visualised with corresponding variables  $a$  for the width of a ridge and  $b$  for the space between two ridges.

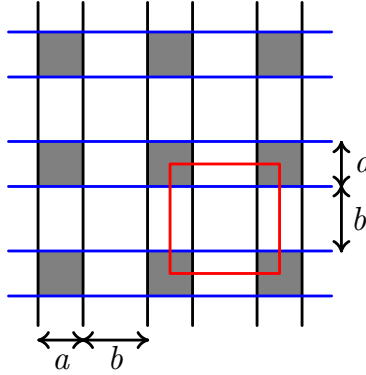


**Figure 5:** Approximation of the contact area for  $\alpha = 90^\circ$ , the contact areas are shaded. Note that the contact areas are squares of length  $a$  as a result of the two coating layers being identical. This situation can also be seen in Figure 2 (c). The red lines describe a periodic unit cell.

Assuming the force is uniformly distributed,  $F_f$  can also be written as

$$F_f = \tau_{\max} A_{\text{eff}}. \quad (2)$$

In here  $\tau_{\max}$  is the maximal traction, which a property that is determined by the material type and condition.  $A_{\text{eff}}$  is the effective contact area.

In Figure 4, 5 and 6 the relevant variables and contact shapes of this problem are visualised.

The typical width of a ridge is  $a$ , whereas the distance between the sides of two ridges is labeled  $b$ . The contact area in case of a finite, flat surface on top of an infinite plate, i.e. in absence of protrusions, is simply the area of the finite surface. This same area will be known as the apparent area,  $A_{\text{app}}$ , in cases deviating from a flat surface, i.e. a surface with a roughness. In this problem the apparent area is, unlike the effective area, independent of the orientation angle making it a constant. The macroscopic length of the square plate that was used in experiments is labeled  $L$ , making  $A_{\text{app}}$  equal to  $L^2$ . To see how the

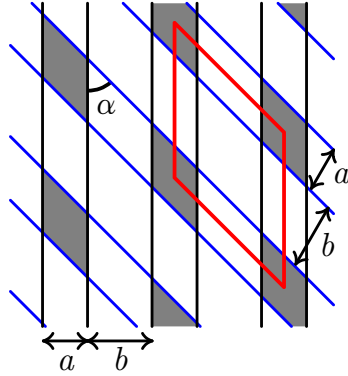


**Figure 6:** The contact areas with ridge orientations differing by angle  $\alpha$ . The shaded regions are contact regions and a unit cell is defined by the red lines. This is another way of showing the setup in Figure 2 (a).

contact area is constructed from micro-scale to macro-scale, several equations are presented, the first of these is

$$A_{\text{app}} = L^2 = N_{90}(a + b)^2. \quad (3)$$

In the equation above the apparent area is written as a rational number times the area of one unit cell in case of  $90^\circ$ , see the red lines in Figure 5 for the depiction of a unit cell. In this case the number of contact areas is simply the number of touching ridges in one dimension times the number of touching ridges in the other dimension,

$$N_{90} = \frac{L^2}{w^2}, \quad (4)$$

where  $w$  equals  $a + b$ . As the apparent area does not depend on the angle an expression similar to (3) can be made for an angle other than  $90^\circ$ , now with a unit cell as defined in Figure 6:

$$A_{\text{app}} = L^2 = N_\alpha \frac{(a + b)^2}{\sin(\alpha)}. \quad (5)$$

In (5) we have made use of the fact that the area of a parallelogram is equal to a side times the respective height. The respective height is  $w$ , with regards to the side of  $w_\alpha$ , which is  $w/\sin(\alpha)$ . Equating (3) and (5) gives us the following expression for the number of unit cells at any angle:

$$N_\alpha = N_{90} \sin(\alpha). \quad (6)$$

Looking at (5) and Figure 5, it can be seen that the effective contact area,  $A_{\text{eff}}$ , follows

$$A_{\text{eff}} = N_\alpha \frac{a^2}{\sin(\alpha)}. \quad (7)$$

Variable	Symbol	Value
Length of coating	$L$	$1.0 \times 10^{-1}$ m
Ridge width	$a$	$1.4 \times 10^{-4}$ m
Space between ridges	$b$	$2.0 \times 10^{-4}$ m
Length of 1 period	$w$	$3.4 \times 10^{-4}$ m
Number of contact areas at $90^\circ$ alignment	$N_{90}$	$8.7 \times 10^6$

**Table 1:** Variables describing rectangular protrusions with corresponding typical values, for illustration of variables see Figures 4,5 and 6.

If one now looks back at (6), it can readily be seen that the angular dependence of  $A_{\text{eff}}$  drops out, combining (4), (6) and (7) we are left with

$$A_{\text{eff}} = \frac{L^2 a^2}{(a + b)^2}. \quad (8)$$

This model, in which rectangular undeformable protrusions were assumed, could not predict anisotropic behaviour. The contact area this model yields is a constant, depending only on the microscopic dimensions of the actuated liquid crystal polymer layer. This constant is given as  $A_{\text{eff}} = L^2 a^2 / (a + b)^2$ . Filling in the values from Table 1 results in an effective contact area of 17% of the apparent area.

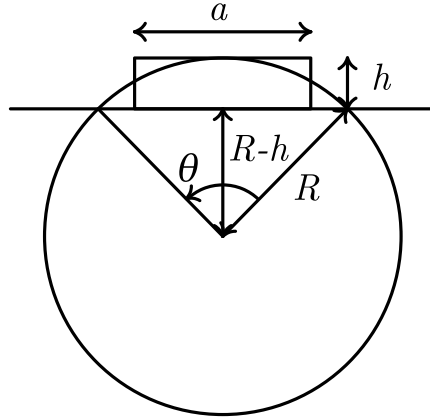


**Figure 7:** Relevant dimensions in modelling ridges as part of a cylinder.

## 4 Cylindrical protrusions model

To take deformation into account, additional theory is needed. The field of contact mechanics studies the deformation of solids that touch each other at one or more points. A problem that arises when one attempts to create a model in which deformation is incorporated is that analytical expressions are only available for a small range of simple geometries, of which a contact between rectangular ridges is not one. Due to this limitation, the second model in this paper approximates the protrusions as being part of a cylinder that is being indented. This idea is illustrated with relevant lengths in Figure 7. In approximating ridges as cylinders two variables are available, the height of the ridges  $h$  with respect to the surface and the width of a ridge  $w$ . Their respective values of  $1.2 \times 10^{-6}$  m and  $3.4 \times 10^{-4}$  m have been determined using data from interferometer measurements <sup>[10]</sup>, see Figure 1. As  $h \ll a$ , our region of interest will up to some extent resemble the first model, however a larger force will now result in a larger area of contact as one would expect. This approximation of the ridges preserves the average height and volume of a real ridge, but not the width. The ridge volume is preserved if the right value of the cylinder radius,  $R$ , is chosen. This is true if

$$A_{\text{seg}} = wh, \quad (9)$$

where  $A_{\text{seg}}$  is the cross sectional area of the protrusion, this is nearly the case in Figure 7. An expression for  $A_{\text{seg}}$  is given by

$$A_{\text{seg}} = A_{\text{sec}} - A_{\text{tri}}. \quad (10)$$

In here  $A_{\text{sec}}$  is the area of the section of the circle and  $A_{\text{tri}}$  is the area of the two right angled triangles as seen in Figure 7. The angle  $\theta$  is defined as the angle spanned by the protrusion. The following equations provide an expression which

will be used to find  $R$ :

$$\theta = 2 \cos^{-1} \left( \frac{R-h}{R} \right), \quad (11)$$

$$A_{\text{sec}} = \frac{\theta R^2}{2} \quad (12)$$

and

$$A_{\text{tri}} = (R-h) R \sin \left( \frac{\theta}{2} \right). \quad (13)$$

Substituting (11) in (12) and (13) and filling these into (10) leaves us with an  $R$  of  $4.6 \times 10^{-3}$  m.

One of the most basic models for predicting contact between deformable surfaces derives from the work of Hertz<sup>[11]</sup>. At this point in time more sophisticated models have been proposed which take into account adhesion and some other factors which are missing in the Hertzian model. All of these models, however, require additional information on surface energies, average Lennard-Jones potentials and other terms which are not available at this time, that is why this model makes use of the contact theory by Hertz. This gives an approximation which is sufficient for the purpose of this paper. A full derivation of the theory that is needed to describe contact between cylinders of equal radius at different angles is too long for the purpose of this paper. Therefore a short introduction to the relevant theory and variables is given, but a full derivation can be found in chapter 4 of Johnson's Contact Mechanics<sup>[12]</sup>.

When the protrusions are aligned parallel a series of line contacts appear. To describe the contact area the semi-contact-width  $c$  is used:<sup>[12]</sup>

$$c = \left( \frac{4PR^*}{\pi E^*} \right)^{\frac{1}{2}}. \quad (14)$$

In here the total load acting on one contact area,  $P$ , is given by the total force divided by the number of line contacts  $N_{\text{par}}$ , so that

$$P = \frac{F_{\text{N}}}{N_{\text{par}}}, \quad (15)$$

where  $N_{\text{par}}$  equals  $L/w$ .  $R^*$  is the relative curvature of the contact region, which follows

$$\frac{1}{R^*} = \frac{1}{R_1} + \frac{1}{R_2}, \quad (16)$$

with both  $R_1$  and  $R_2$  equal to the cylinder radius  $R$ . Finally  $E^*$  is the reduced modulus, given by

$$\frac{1}{E^*} = \frac{1-\nu_1^2}{E_1} + \frac{1-\nu_2^2}{E_2}. \quad (17)$$

The resulting total contact area  $A_{\text{eff}}$  for this setup follows

$$A_{\text{eff}} = 2cLN_{\text{par}}. \quad (18)$$

Physical quantity	Symbol	Value
Height of ridge	$h$	$1.2 \times 10^{-6}$ m
Cylinder radius	$R$	$4.6 \times 10^{-3}$ m
Normal force	$F_N$	1 N
Poisson ratio	$\nu$	0.4
Young's modulus	$E$	1 GPa
Number of contact areas at $0^\circ$ alignment	$N_0$	$2.9 \times 10^3$

**Table 2:** Variables and their typical values for the deformable cylinder model.

When the protrusion alignment is orthogonal, contact circles are formed of which the radius is given by<sup>[12]</sup>

$$c = \left( \frac{3PR}{4E^*} \right)^{\frac{1}{3}}. \quad (19)$$

The total contact area now follows

$$A_{\text{eff}} = \pi c^2 N_{90}. \quad (20)$$

When the protrusions are aligned at an angle between  $0^\circ$  and  $90^\circ$ , the shape of the contact is an ellipse. When  $d$  is the major semi-axis and  $e$  is the minor semi-axis of the ellipse, the area can be calculated using<sup>[12]</sup>

$$f = (de)^{\frac{1}{2}} = \left( \frac{3PR_e}{4E^*} \right)^{\frac{1}{3}} F(R'/R''), \quad (21)$$

with  $R'$  and  $R''$  being the radii of curvature near the contact, these are related to  $R_e$ , or the equivalent radius of curvature by

$$R_e = (R'R'')^{\frac{1}{2}}. \quad (22)$$

Then  $F(R'/R'')$  is a function of elliptic integrals, to calculate  $R_e$  and  $F(R'/R'')$  for every angle additional steps and theory are needed, these can be found in contact theory books. For the derivation of the cited formulae above, see chapter 4 of Contact mechanics by Johnson<sup>[12]</sup>.

This second model, where deformation plays a role, does show an angular dependence. The calculated areas of contact as a function of the angle can be seen in Figure 8. The values of the used variables can be found in Table 2.

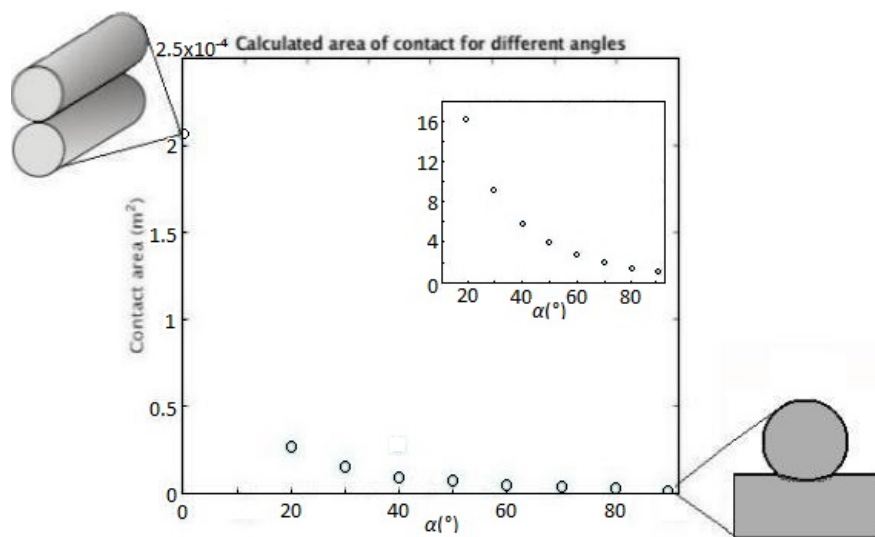


**Figure 8:** This figure shows the calculated angular dependence of the contact area for the cylinder model. In the inset figure the calculated area has been normalised with respect to the orthogonal alignment value. The calculated area corresponding to parallel alignment has been omitted in the inset. The resulting inset figure is easier to compare to Figure 2 (d).

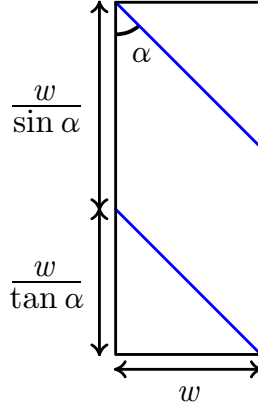


**Figure 9:** A limiting case for the rectangular protrusions model is depicted. One unit cell now exactly fits in a plate.

## 5 Discussion

### 5.1 Rigid rectangular protrusions model

The experimental friction coefficient<sup>[10]</sup> as a function of the angle is seen Figure 2 (d) and can be used to compare with the behaviour of the models proposed in Sections 3 and 4. In the results of the first model it was found that the contact area is independent of the angle, however, one can readily see that when the protrusions are perfectly aligned, the contact area is not given by the expression which is presented in the results, this problem is now examined. As  $\alpha$  goes to 0, the amount of unit cells goes to 0. This is because our definition of a unit cell loses its significance when it no longer fits in a macroscopic plate, this happens when  $\alpha$  is sufficiently small. The moment in which this starts to happen has been depicted in Figure 9. This tells us that unit cells provide us with useful information as long as the following holds:

$$\frac{w}{\sin(\alpha)} + \frac{w}{\tan(\alpha)} \leq L. \quad (23)$$

Which can be written as

$$w \frac{1 + \cos(\alpha)}{\sin(\alpha)} \leq L. \quad (24)$$

Using a value of 0.1 m for  $L$  and a value of  $3.4 \times 10^{-4}$  m for  $w$ , the above is true for any  $\alpha$  larger than  $0.39^\circ$ , so for any angle larger than this we can predict a contact area. However, comparing this result to the experimental results it is immediately evident that this model does not cover the angular dependence of the friction coefficient.

## 5.2 Cylindrical protrusions model

The second model seems more promising, as at a first sight a curve through the points in Figure 8 seems similar to experimental results. However, a major difference in the ratios of the contact areas at different angles becomes apparent when the result is normalised with respect to the contact area at  $90^\circ$ , see the inset in Figure 8. Some of the approximations made in calculating the contact area in the cylindrical protrusions model do not hold for  $\alpha$  close to zero. For this reason the data point for  $90^\circ$  in the inset figure has been omitted. Comparison of Figures 2 and 8 suggests that friction force may be area dependent, but that another mechanism is dominant in determining the friction coefficient. It is also that there are shapes which have a better resemblance of the protrusions in the actuated LC polymer layer. It is, however, likely that no analytical solution can be obtained for these shapes and that another mechanism than pure contact is needed to solve the problem at hand. Interlocking of the ridges may be the mechanism that can explain the angle dependence of the friction coefficient.

## 5.3 Friction mechanisms

Recalling that the initial problem concerns explaining the friction coefficient,  $\mu$ , it may initially seem logical to investigate the contact area and relate this to the friction force. The desired result would be a curve describing the contact area which has a good resemblance of Figure 2 (d). In this approach, it is assumed there is a linear relation between contact area and friction. Further investigation, however, reveals that a pressure distribution needs to be calculated over the contact area in order to find the friction force. As the calculated contact area cannot explain the friction behaviour, it is logical to look if there are other mechanisms which may determine the measured friction. A possible friction mechanism is that of interlocking, which can be visualised by gears fitting into each other. Looking at Figure 3, the middle curve describes the friction if no protrusions are formed. In this situation one would assume that the contact area is maximal. Seeing that the measured friction increases by a factor of 1.5 when protrusions are aligned parallel, the conclusion arrives that the contact area does indeed not play a dominant role in this case. Looking into the concept of interlocking it becomes apparent that there are no analytical expressions readily available for the problem at hand. In an attempt to quantify the contribution of interlocking to the measured friction, it can be assumed that friction force at every scale is determined by different mechanisms with their own contribution to the total friction. Furthermore the relative contribution of each of these mechanisms can be a function of the length scale and the material properties of a problem. Then it can be assumed that there are two mechanisms that dictate the friction behaviour, the first of these being Coulomb interaction. Even in the case of a perfectly smooth surface, Coulomb interaction would still need to be overcome in order to allow movement, making this one of these friction mechanisms. In case of surface roughness, material needs to deform in order to allow movement, so that the overcoming of Lennard-Jones potentials is a logic second

friction mechanism that has a major contribution to the measured friction. The overcoming of Lennard-Jones potentials can be an analogy for interlocking at the smallest length scales. This then means that the three curves in Figure 3 each have different contributions of these two mechanisms, for which we can make an educated guess if the experiments of Liu and Broer are repeated with different values for the parameters  $a, b$  and  $F_N$ .

#### 5.4 Numerical model

After finishing the cylindrical protrusions model, some effort was made to see whether a numerical solution of the contact area would yield better results than the analytical model, especially for angles closer to  $90^\circ$ , where the analytical approximation is less accurate. In one of the last stages of building this model, the prescribed displacement of the top face was directly set as the input parameter for the numerical model to obtain the normal force, as a comparison to the experimental data. The computational results indicated that the displacement of the top square slab had become so large that the protrusions were completely compressed into the material, meaning that the contact area will be equal to the total, apparent area. This means using the normal forces used in the experiments as direct input to this numerical model of cylinder contact cannot reproduce the experimental results. Adjusting the mesh size resulted in even larger differences between the prediction and the experiments. Because the results from the numerical model did not correspond to a situation which is physically possible, the details of the numerical modelling and processing have been omitted from this report. If a virtual displacement field is prescribed to the top surface, so that the top plate is not fully compressed and that the resulting reaction force is also smaller than in the experiments, the profile seen in figure 10 is achieved. Since this elliptical shape is also proposed by theory, it is assumed that the discrepancy arises due to a scaling problem.

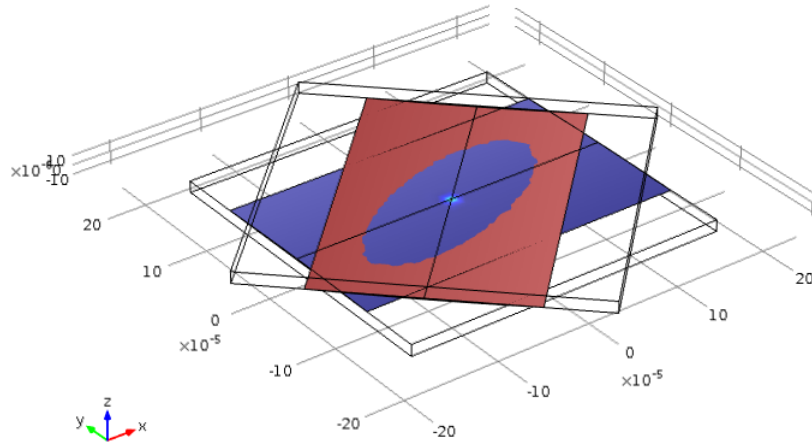


**Figure 10:** The numerically derived contact area as two cylinders are pressed onto each other at an angle is seen. The normal force  $F_N$  resulting from the prescribed displacement is orders of magnitude smaller than the force in the experiments of Liu and Broer. This model was designed in COMSOL.

## 6 Conclusion

It can be concluded that approximating the surface patterns in a liquid crystal polymer layer by rigid rectangular protrusions results in a contact area that is independent of the angle between the coatings. As this first model does not capture the experimentally seen anisotropic friction behaviour, a second model was proposed. The second model analytical model describes the protrusions as being deformable and cylindrical, the results of this model do have an angular dependence. However, a different mechanism must be dominant as the difference between the result from this model and the experiment are too large. This suggests that a future research into the interlocking mechanism is needed to fully explain the anisotropic friction coefficient. Suggestions for this include either directly building a numerical model that can explain the process of interlocking, or creating a workaround which describes friction as a sum of two mechanisms, for which values can be determined by more experiments.

## References

- [1] U. Pettersson and S. Jacobson. Textured surfaces for improved lubrication at high pressure and low sliding speed of roller/piston in hydraulic motors. *Tribology International*, 40(2):355–359, 2007.
- [2] Antonis I Vakis Soheil Solhjoo. Definition and detection of contact in atomistic simulations. *Computational Materials Science*, 109(11):172–182, 2015.
- [3] L.Heepe M.J. Baum and S.N. Gorb. Dry friction of microstructured polymer surfaces inspired by snake skin. *Beilstein Journal of Nanotechnology*, 5(83):1091–1103, 2014.
- [4] Z. Dai W. P. King R. W. Carpick C. Greiner, J. R. Felts. Local nanoscale heating modulates single-asperity friction. *Nano letters*, 10(11):4640–4645, 2010.
- [5] M.-H. Li. Artificial muscles based on liquid crystal elastomers. *The Royal Society*, 364(1847):2763–2777, 2006.
- [6] F. Reinitzer. *Beiträge zur kenntniss des cholesterins*. Monatsh. Chem. 9, 1888.
- [7] S. Zumer D. J. Broer, G. P. Crawford. *Cross-Linked Liquid Crystalline Systems*. CRC Press, 2011.
- [8] Q. Li. *Liquid Crystals Beyond Displays*. John Wiley & Sons, 2012.
- [9] Timothy J. White and Dirk J. Broer. Programmable and adaptive mechanics with liquid crystal polymer networks and elastomers, 2015.
- [10] D. Liu and D. J. Broer. Light controlled friction at a liquid crystal polymer coating with switchable patterning, 2014.
- [11] H. Hertz. *Über die Berührung fester elastischer Körper*. Journal für die reine und angewandte Mathematik, 1881.
- [12] K. L. Johnson. *Contact mechanics*. Cambridge University Press, 1985.